

1 **VERTICAL FACING PANEL-JOINT GAP ANALYSIS FOR STEEL-**  
2 **REINFORCED SOIL WALLS**

3

4 I.P. Damians<sup>1</sup>

5 R.J. Bathurst<sup>2</sup> (corresponding author)

6 A. Lloret<sup>3</sup>

7 A. Josa<sup>4</sup>

8

9

---

<sup>1</sup> Ph.D. Candidate, Department of Geotechnical Engineering and Geo-Sciences (ETCG) and Institute for Sustainability (IS.UPC). Universitat Politècnica de Catalunya-BarcelonaTech (UPC), Spain; Phone: (+34) 93 401 1695, Fax: (+34) 93 401 7251, E-mail: [ivan.puig@upc.edu](mailto:ivan.puig@upc.edu)

<sup>2</sup> Professor, GeoEngineering Centre at Queen's-RMC, Civil Engineering Department, 13 General Crerar, Sawyer Building, Room 3417 Royal Military College of Canada Kingston, Ontario K7K 7B4, Canada; Phone: (+1) 613 541 6000 ext, 6479, Fax: (+1) 613 541 6218, E-mail: [bathurst-r@rmc.ca](mailto:bathurst-r@rmc.ca)

<sup>3</sup> Professor, Department of Geotechnical Engineering and Geo-Sciences (ETCG). Universitat Politècnica de Catalunya-BarcelonaTech (UPC), Spain; Phone: (+34) 93 401 6870, Fax: (+34) 93 401 7251, E-mail: [antonio.lloret@upc.edu](mailto:antonio.lloret@upc.edu)

<sup>4</sup> Professor, Department of Geotechnical Engineering and Geo-Sciences (ETCG) and Institute for Sustainability (IS.UPC). Universitat Politècnica de Catalunya-BarcelonaTech (UPC), Spain; Phone: (+34) 93 401 7260, Fax: (+34) 93 401 7251, E-mail: [alejandro.josa@upc.edu](mailto:alejandro.josa@upc.edu)

**Abstract**

10  
11  
12  
13  
14  
15  
16  
17  
18  
19  
20  
21  
22  
23  
24  
25  
26  
27  
28  
29  
30  
31  
32  
33  
34  
35  
36  
37  
38  
39  
40

This paper reports the results of a numerical parametric study focused on the prediction of vertical load distribution and vertical gap compression between precast concrete facing panel units in steel reinforced soil walls ranging in height from 6 m to 24 m. The vertical compression is accommodated by polymeric bearing pads placed at the horizontal joints between panels during construction. The paper demonstrates how gap compression and magnitude of vertical load transmitted between horizontal joints are influenced by joint location along the height of the wall, joint compressibility, and backfill and foundation soil stiffness. The summary plots in this study can be used to estimate the number and type (stiffness) of the bearing pads to ensure a target minimum gap thickness at the end of construction, demonstrate the relative influence of wall height and different material component properties on vertical load levels and gap compression, or used as a benchmark to test numerical models used for project-specific design. The paper also demonstrates that while the load factor (ratio of vertical load at a horizontal joint to weight of panels above the joint) and joint compression are relatively insensitive to foundation stiffness, the total settlement at the top of the wall facing is very sensitive to foundation stiffness. The paper examines the quantitative consequences of using a simple linear compressive stress-strain model for the bearing pads versus a multi-linear model which is better able to capture the response of bearing pads taken to greater compression. The study demonstrates that qualitative trends in vertical load factor are preserved when a more advanced stress-dependent stiffness soil hardening model is used for the backfill soil compared to the simpler linear-elastic Mohr-Coulomb model. While there are differences in vertical loads and gap compression using both soil models for the backfill, the differences are small and not of practical concern.

**CE Database subject headings:** Retaining structures; Reinforcing steel; Panels; Finite element method.

**Author keywords:** Soil retaining walls; Steel reinforcement; Vertical loads; Facing panels; Bearing pads; Finite element modeling.

## 41 Introduction

42

43 Steel reinforced soil walls constructed with steel strips, bar mats or steel ladders that are attached  
44 to steel-reinforced concrete panels are a mature technology. The design focus in guidance  
45 documents used by geotechnical engineers is most often on the internal and external stability of  
46 the gravity mass formed by the facing panels and reinforced soil zone (e.g., **AASHTO 2014**).  
47 However, the facing column is an important structural component of these systems. It must be  
48 designed to carry vertical loads that are greater than the self-weight of the panels. **Damians et al.**  
49 **(2013)** collected data from instrumented steel reinforced soil walls and found that the ratio of  
50 measured vertical load to panel self-weight (load factor) ranged from about 2 to 5. These  
51 additional vertical loads are the result of downdrag forces generated by backfill soil-panel  
52 interface shear due to relative settlement of the backfill plus parasitic downward loads generated  
53 at the connections between the steel soil reinforcement elements and the back of the facing  
54 **(Figure 1)**. The relative stiffness of the backfill soil and the horizontal joint (bearing pad)  
55 stiffness will influence the magnitude of downdrag loads acting at the wall face and connections.  
56 If vertical downdrag loads are excessive and/or joint stiffness is too low, then the panels can  
57 come into contact leading to spalling and/or failure of the concrete panels. Documented  
58 examples of these types of failures are given in the paper by **Damians et al. (2013)**. While panel  
59 facing damage due to loss of gap space is visually detectable it does not typically threaten the  
60 overall stability of the structure. For this reason when it does occur, it is ranked as moderately  
61 significant based on a post-construction inspection and performance assessment protocol  
62 developed in the USA (**Gerber 2012**) even though wall appearance may be unsatisfactory to the  
63 observer.

64

65 In an earlier related study, the writers carried out a numerical parametric analysis to investigate  
66 the influence of joint compressibility, reinforced soil stiffness and foundation stiffness on  
67 vertical panel loads and gap compression using the case of a single wall of height  $H = 16.7$  m  
68 **(Damians et al. 2013)**. The parameters varied were joint axial stiffness (compressibility due to  
69 the number and type (stiffness) of the bearing pads), backfill soil and foundation stiffness. The  
70 numerical modelling was carried out using the program **PLAXIS (2008)** together with simple  
71 linear elastic-plastic constitutive models for the component materials. The same finite element

72 modeling package with the same constitutive models for the component materials and interfaces  
73 has been used to satisfactorily reproduce the behavior of an instrumented 16.7 m-high steel strip  
74 reinforced soil wall (**Damians et al. 2015**). Lessons learned regarding the use of program  
75 PLAXIS to model reinforced soil walls with discontinuous reinforcement layers can be found in  
76 the papers by **Yu et al. (2015a, b)**.

77

78 The numerical simulation results reported by **Damians et al. (2013)** also confirmed physical  
79 measurements mentioned earlier that the magnitude of the vertical load between panels was  
80 always greater than the panel self-weight above the joint. The ratio of vertical load to panel self-  
81 weight (load factor) ranged from about 2 to 7 depending on the relative joint stiffness and the  
82 relative stiffness of the backfill soil and the foundation soil in their numerical simulations. The  
83 numerical simulation results for  $H = 16.7$  m and interface friction coefficient  $R = 0.3$  were  
84 shown to be consistent with computed load factors from field measurements in the range of  
85 about 2 to 5 for joint stiffness values of about 0.1 to 1.1 MPa/m.

86

87 The paper by **Damians et al. (2013)** is an important start to identify issues related to joint  
88 compressibility and design, and to demonstrate the influence of wall joint compressibility and  
89 stiffness of the backfill soil and foundation on vertical loads developed in the concrete panel  
90 facing units of steel reinforced soil walls. However, this earlier work was limited to a single wall  
91 height and simple constitutive models and assumptions for the component materials (e.g. linear  
92 elastic models with Mohr Columb failure criterion for the soil and linear elastic reinforcement).  
93 Furthermore, numerical outcomes were restricted to the bottom (most critical) joint without  
94 reporting the behavior of the horizontal joints along the entire height of the wall. Questions  
95 remain regarding possible differences in the quantitative results and qualitative trends reported in  
96 this earlier study with respect to other wall heights. To answer these questions, numerical  
97 simulation of walls with height  $H = 6, 12, 18$  and  $24$  m were carried out and their performance  
98 summarized. In addition, the influence of constitutive model type for the backfill soil and load-  
99 compression behavior of the bearing pads is also explored in more detail.

100

## 101 **Bearing Pads**

102

103 A detailed explanation of the role of the polymeric bearing pads that are placed at the horizontal  
104 joints between the concrete panels in steel reinforced soil walls can be found in the paper by  
105 **Damians et al. (2013)**. A brief summary of the important points is repeated here for  
106 completeness.

107

108 The primary functions of bearing pads are to act as spacers to: 1) transfer vertical load between  
109 the concrete facing panels; 2) accommodate possible differential settlements between the backfill  
110 and the facing; and, 3) prevent contact between the panels. In the USA a minimum gap of  
111 thickness of 12 mm is recommended after the wall is constructed (**Berg et al. 2009**). In the UK  
112 the recommended minimum gap thickness is 1/150 of the panel height (**BSI BS8006 2010**).  
113 Hence, for a panel height of 1.5 m (the case in this study) the minimum gap thickness at end of  
114 construction is 10 mm. Clearly, to meet these performance criteria the number of bearing pads  
115 (typically a minimum of two), stiffness (compressibility) and thickness of the bearing pads  
116 (typically 20 – 25 mm) are of primary importance. The most common bearing pad materials are  
117 EPDM (ethylene propylene diene monomer) and HDPE (high density polyethylene).  
118 Measurements of gap closure have been reported in the literature. **Finlay (1978)** reported a  
119 maximum closure of 10 mm for a 6.3 m-high section of wall and **Choufani et al. (2011)** reported  
120 20 mm of gap closure for a 20 m-high wall constructed with 25 mm-thick bearing pads.

121

## 122 **Numerical Model Details**

### 123 ***General***

124

125 The 2D finite element method (FEM) program **PLAXIS (2008)** was used to carry out the  
126 numerical simulations in this study. **Figure 2** shows the finite element mesh (15-node triangle  
127 elements) and geometry adopted in the analyses. Four wall heights were considered  
128 corresponding to  $H = 6, 12, 18$  and  $24$  m. The foundation depth was kept constant at  $D = 25$  m.  
129 In a related study, the writers investigated the influence of relative foundation compressibility on  
130 performance of reinforced walls having a range of backfill and reinforcement stiffness (**Damians  
131 et al. 2014**). In this previous study, the foundation was treated as equivalent linear Winkler  
132 springs with stiffness computed as  $k = E/D$  where  $E$  is the Young's modulus of the foundation  
133 soil. In addition, the foundation stiffness varied from  $k = 4$  MPa/m to rigid corresponding to

134 medium loose sand to intact rock (**Bowles 1996**). In the current study,  $k = 0.4$  to  $400$  MPa/m  
135 corresponding to clay to weathered rock. The lower limit was purposely selected to capture  
136 trends in numerical outcomes corresponding to the low end of foundation stiffness. The  
137 reinforcement length ( $L$ ) was taken as  $0.7$  times the wall height in all cases, and the embedment  
138 depth was  $0.1 \times H$ . These values satisfy minimum criteria in the USA for the wall heights and  
139 geometry in this study (**Berg et al. 2009**).

140

141 The vertical domain boundaries were fixed in the horizontal direction. The bottom boundary was  
142 fixed in both horizontal and vertical directions. The model domain (depth and width) and  
143 numerical mesh element refinement were selected to jointly optimize computation time and  
144 minimize the influence of problem boundaries. Smaller numerical mesh elements were generated  
145 in the soil zone immediately in front of the wall toe and in zones adjacent to all reinforced-soil  
146 interfaces and horizontal panel joints. Each numerical wall was built incrementally from the  
147 bottom up to simulate construction in the field.

148

149 In the sections to follow, the properties of the component materials and their implementation  
150 within the PLAXIS program are the same as those reported in the paper by **Damians et al.**  
151 (**2013**), unless noted otherwise. Hence, some details in the sections to follow are omitted for  
152 brevity.

153

### 154 ***Material Properties and Interfaces***

155

156 *Soil* (backfill and foundation): Material properties for the soil zones (backfill and foundation) are  
157 summarized in **Table 1**. The soil materials in the majority of simulations are modeled as elastic-  
158 plastic materials using the Mohr-Coulomb failure criterion. For simplicity, no attempt has been  
159 made to simulate compaction effects during placement of soil layers. The ratio of soil elastic  
160 modulus for different soil material zones (e.g., backfill soil and foundation) has been kept  
161 constant between matching simulations that vary only with respect to wall height. In this study,  
162 the backfill stiffness  $E_{(\text{backfill})}$  refers to the soil at  $1$  m and greater from the back of the concrete  
163 panels. At closer distances the soil stiffness is reduced by  $50\%$  (**Table 1**). This was done to  
164 capture the effect of less compaction energy on soil stiffness using lighter compaction equipment

165 which is recommended practice immediately behind the wall face to minimize additional  
166 compaction-induced loads on the concrete facing panels (**Berg et al. 2009**). The focus of the  
167 paper is on the influence of relative compressibility of the joint inclusions, backfill soil zone and  
168 foundation soil on wall facing behavior. Hence, a large cohesive strength component (50 kPa) for  
169 the foundation soil was adopted to ensure that deformations originating in the foundation soil  
170 were within the elastic range of the soil (i.e., working stress conditions) and thereby simplify the  
171 interpretation of results

172

173 **Huang et al. (2009)** and **Damians et al. (2014)** demonstrated that the use of more complex non-  
174 linear multi-parameter soil constitutive models does not guarantee improved numerical accuracy  
175 with measured wall performance. Nevertheless, a number of wall cases were repeated using the  
176 hardening soil model that is available in PLAXIS in order to examine the sensitivity of numerical  
177 outcomes to choice of soil constitutive model for the backfill soil. Hardening model parameters  
178 are given in **Table 1**. Details of the model can be found in the PLAXIS software manual  
179 (**PLAXIS 2012**). The  $E_{50}^{ref}$  value for the hardening soil model was selected to match the elastic  
180 modulus of the soil in the corresponding elastic analyses and the same M-C failure criterion was  
181 also adopted. The default value of  $R_f = 0.9$  in program PLAXIS was used in this study. For  
182 project-specific design a lower value may be appropriate (e.g.,  $R_f = 0.75$ ) based on fitting to  
183 triaxial compression testing of site-specific soils as demonstrated by **Damians et al. (2014)**.  
184 However, in the current study the numerical outcomes were found not to be sensitive to the  
185 choice of  $R_f$  in the range of 0.75 to 0.9 which is likely because the soils remained largely in the  
186 working stress (elastic) range. It should be noted that minor soil yielding occurred in a very thin  
187 column at the back of the facing, at the foundation toe and at the back of the reinforced soil zone  
188 in some simulations with both M-C and hardening soil models. However, large and contiguous  
189 soil failure zones in the reinforced soil mass consistent with conventional notions of reinforced  
190 soil wall failure did not occur in any simulations.

191

192 *Facing* (concrete panels and bearing pads): The material properties assumed for the precast  
193 concrete facing panels and the polymeric bearing pads (horizontal joints) are shown in **Table 2**.  
194 The joint axial stiffness was computed based on plan area of each pad, pad modulus and the  
195 number of pads per 1.5 m-long panel joint. These calculations result in an initial linear

196 compression response of the joints as a result of the compressive stress-strain behavior of the  
197 individual pads (**Figure 3**). The assumption of linear joint stiffness also simplifies parametric  
198 analyses to isolate the influence of the compressibility of the horizontal joints between facing  
199 panels, wall height and reinforcement layer location on vertical loads transmitted through the  
200 wall facing. For walls with a large number of very stiff bearing pads, the assumption of linear  
201 compression is reasonable for in-service (operational) conditions. For walls with more  
202 compressible joints, the assumption of linear compression is satisfactory if compression is  
203 restricted to (say) 10% for HDPE pads and (say) 40% for EPDM pads based on published data  
204 (**Neely and Tan 2010; Choufani et al. 2011**). In the simulations to follow, the bearing pads  
205 were assumed to have an initial thickness of  $t = 20$  mm (**Table 2**). The minimum available gap  
206 space is taken as 20 mm by assuming that the gap at the concrete panel lip(s) is at least equal to  
207 20 mm (**Figure 1**).

208

209 *Reinforcement:* The reinforcement layers were placed at uniform vertical spacing of 0.75 m in  
210 each wall and each layer was assigned a constant axial stiffness (J) (**Table 3**). The axial stiffness  
211 was increased with depth below the top of the wall to capture the increase in number of  
212 reinforcing strips in a layer which is common practice for steel strip walls, and/or to capture the  
213 increase in total cross-section area per unit running length of wall that is used in some steel  
214 ladder wall systems constructed with circular bars. The axial stiffness values vary from about  $J =$   
215 30 MN/m to 100 MN/m for wall heights of  $H = 6$  to 24 m, respectively. These values are  
216 consistent with the range of values reported by **Bathurst et al. (2011)** for steel grid reinforced  
217 soil walls and **Huang et al. (2012)** for steel strip reinforced soil walls.

218

219 *Interfaces:* In the earlier preliminary study by **Damians et al. (2013)**, a sensitivity analysis was  
220 carried out using a range of interface friction coefficient  $R = \tan \delta / \tan \phi$  where  $\delta$  is soil-concrete  
221 panel interface friction angle and  $\phi$  is the friction angle of the backfill soil. The best value was  
222 determined to be  $R = 0.3$  based on comparison of predicted vertical toe loads with measured  
223 results from an instrumented field wall (**Runser et al. 2001; Damians et al. 2014**), and thus is  
224 the value used in the current study. The soil-reinforcement interaction was modeled assuming a  
225 perfect bond behavior (i.e.,  $R = 1$ ). This value is consistent with measured pullout test data for



226 ribbed steel strips and well compacted granular soils reported in the literature (**Schlosser and**  
227 **Elias 1978; Miyata and Bathurst 2012; Bathurst et al. 2011**).

228

## 229 **Results of Analyses**

### 230 ***Influence of Joint Stiffness and Soil Stiffness on Vertical Facing Panel Loads***

231

232 Numerical results using linear axial (compressive) joint stiffness are reported first. **Figure 4**  
233 shows load factor (ratio of measured vertical toe load to sum of panel self-weights) plotted  
234 against depth of joint below the top of the wall for four different wall heights, two joint  
235 materials, and four different combinations of backfill and foundation stiffness. The soil  
236 constitutive models are linear elastic with M-C failure criterion in all cases. For reference  
237 purposes, the data for cases with  $H = 18$  m are quantitatively similar to previously reported  
238 results in the earlier related paper by **Damians et al. (2013)**. Only numerical results in which  
239 there was a positive gap are presented. No attempt was made to simulate the concrete-to-concrete  
240 contact condition, which in practice should be avoided. The plots also show the load factor at  
241 which 10% and 40% compression of the joint is exceeded. These values correspond to the first  
242 break point in the compressive stress-strain plots for the HDPE and EPDM bearing pads shown  
243 in **Figure 3**. Hence, the plots in **Figure 4** assume that the initial linear elastic behavior of the  
244 bearing pads persist at all compressive strains. The grey symbols in the figure identify numerical  
245 outcomes where the compression of the bearing pads has extended beyond the initial linear  
246 stress-strain region in **Figure 3** but the panels are not in contact.

247

248 The influence of the above parameters on load factor magnitude and vertical distribution is  
249 complex. The following observations can be made from **Figure 4**:

250

- 251 1. In general, for the same foundation stiffness condition, decreasing the stiffness of the joint  
252 material (EPDM versus HDPE in these examples) and/or increasing the stiffness of the  
253 backfill soil leads to reduced load factor at similar depths below the top of the wall (compare  
254 **Figure 4a** with **4c**, and **Figure 4b** with **4d**).

- 255 2. For the case of a relatively less stiff backfill soil ( $E_{(\text{backfill})} = 10 \text{ MPa}$ ) (**Figure 4a** and **4b**) there  
256 is generally steadily increasing load factor with depth below the wall regardless of joint  
257 material.
- 258 3. For the relatively stiff backfill condition ( $E_{(\text{backfill})} = 100 \text{ MPa}$ ) the vertical load factor is less  
259 for the stiffer foundation soil case at similar depths (compare **Figure 4c** with **4d**).
- 260 4. For walls with the more compressible joints (EPDM) the vertical load factor becomes more  
261 uniform with depth for increasing backfill soil stiffness and the stiff foundation condition with  
262  $E_{(\text{foundation})} = 1000 \text{ MPa}$  (compare **Figure 4b** with **Figure 4d**). The explanation is that the joint  
263 stiffness for the EPDM cases in this parametric study is similar in magnitude to the backfill  
264 soil. Hence, relative downward movement of the wall facing and backfill soil is less for the  
265 case with  $E_{(\text{backfill})} = 100 \text{ MPa}$ .
- 266 5. For the case of HDPE joint material and  $E_{(\text{backfill})} = 100 \text{ MPa}$  and  $E_{(\text{foundation})} = 10 \text{ MPa}$ , there is  
267 relatively little influence of wall height on the magnitude of load factor (**Figure 4c**).
- 268 6. For many cases the linear-elastic region for the HDPE bearing pads is exceeded. The elastic  
269 strain limit of the EPDM pads is greater and it is for this reason that numerical outcomes  
270 where the elastic limit of the material has not been exceeded are more easily visible in the  
271 figure (e.g., **Figures 4c** and **4d**).

272

273 Two walls cases with linear elastic HDPE and EPDM bearing pads were repeated using the  
274 hardening soil model in PLAXIS for the backfill soil only. This soil model captures non-linear  
275 stress-dependent stiffness behavior of frictional soil materials. The results of simulations using  
276 both soil models are compared in **Figure 5**. To minimize visual clutter, numerical outcomes with  
277 strains greater than the initial elastic limit are not identified. In general, the load factor response  
278 curves are similar to those in **Figure 4** but are shifted to the right indicating that qualitative  
279 features in **Figure 4** are preserved in **Figure 5**. Hence, the PLAXIS soil hardening model  
280 predicts greater vertical load transferred through the facing column than the simpler linear-elastic  
281 plastic model. Since the focus of the paper is largely on the relative performance of the walls  
282 using a range of assumed wall component material properties and wall heights, the quantitative  
283 differences in the response curves in **Figure 5** are judged not to be a practical concern from a  
284 performance point of view.

285

286 However, it is worth noting that the run times were up to six times longer for numerical  
287 simulations using the hardening soil model compared to matching cases using the simpler soil  
288 model. For example, using a desk top computer with an Intel<sup>®</sup> Core 2 Duo Pa8600 (2.40 GHz)  
289 (Intel, Santa Clara, California) central processor, the computer solved wall models with  $H = 24$   
290 m in approximately 20 min for elastic M-C soil model cases and 120 min for the hardening soil  
291 model cases. The numerical results presented hereafter are for simulations carried out using  
292 linear elastic M-C soil models.

293

### 294 ***Influence of Joint Stiffness and Soil Stiffness on Panel-Joint Gap***

295

296 **Figure 6** shows the vertical load factor generated at selected joint locations (depth  $z$ ) for each  
297 wall height ( $H$ ) case versus relative joint stiffness. Relative joint stiffness is calculated as the  
298 ratio of the product of the pad elastic modulus, pad area and number of pads per joint, to the  
299 product of backfill soil stiffness and joint (pad) thickness. In this study  $t = 20$  mm which is a  
300 typical thickness for these pads (**Damians et al. 2013**). As a useful reference, the relative joint  
301 stiffness data points in **Figure 6** are matched to the number of bearing pads manufactured from  
302 HDPE and EPDM materials per 1.5 m-long joint. The plots show that the load factor tends to one  
303 as the stiffness ratio goes to zero (e.g., as axial bearing pad stiffness goes to zero). For relative  
304 joint stiffness values greater than about one the load factor is reasonably constant at each depth  
305 location. A load factor of one is possible (i.e., no downdrag forces) if the compressibility of the  
306 horizontal joint is sufficient to allow the concrete panels to settle with the backfill soil.

307

308 **Figure 7** shows the computed joint gap thickness (at the location of the bearing pads) and axial  
309 (compressive) strain at three normalized depth locations. Three different numbers of EPDM and  
310 HDPE pads per panel joint (2, 4 and 6) were assumed in these calculations. The plots show that  
311 the magnitude of backfill stiffness plays a major role in joint compression. For the same fixed  
312 relative joint stiffness value, the gap compression is less for the stiffer backfill soil condition and  
313 gap closure increases with depth below the top of the wall. The influence of foundation stiffness  
314 is less for cases with relative joint stiffness of (say) 0.5 or greater. Some additional numerical  
315 results are shown for the case of an intermediate value of backfill stiffness ( $E_{(\text{backfill})} = 50$  MPa).

316

317 An alternative presentation of the results of parametric analyses is given in **Figure 8**. Here  
318 isolines of equal gap thickness are plotted for each wall height scenario and different  
319 combinations of backfill and foundation stiffness, and different numbers of EPDM and HDPE  
320 bearing pads. These plots can be used for design to select the minimum number of 20 mm-thick  
321 pads at each horizontal joint location to not exceed a specified minimum gap thickness. The 12  
322 mm- and 5 mm-gap isolines in the figure may be taken as the range of minimum acceptable post-  
323 construction values based on recommendations by **Berg et al. (2009)** and **BSI BS8006 (2010)**,  
324 respectively, and observations by **Choufani et al. (2011)**.

325

### 326 ***Influence of Joint Stiffness and Soil Stiffness on Vertical Facing Settlement***

327

328 **Figure 9** shows computed settlements at the top of the concrete facing for different wall heights  
329 and combinations of other parameter values. Previous figures demonstrate that the magnitude of  
330 load factor is sensitive to joint compressibility and relatively less sensitive to foundation  
331 stiffness. However, the plots in **Figure 9** show that foundation compressibility is much more  
332 important than joint compressibility when settlement of the wall facing (or backfill) is a concern.  
333 Examples when wall settlements are important are where the wall supports or adjoins other  
334 structures.

335

### 336 ***Influence of Bearing Pad Constitutive Model on Gap Thickness Prediction***

337

338 A linear compression law for the joint bearing pads has been adopted in the current study and in  
339 the earlier related paper by **Damians et al. (2013)**. A linear model has the advantage of  
340 simplicity which facilitates comparison and understanding of the contribution of the many  
341 factors that influence vertical load transmission and horizontal panel joint compression in steel  
342 reinforced soil walls. Linear models are satisfactory for very stiff horizontal joints (e.g., large  
343 numbers of bearing pads are used at each joint) and/or the strains are kept within elastic limits  
344 (about 10% for HDPE and 40% for EPDM type). However, the actual compression behavior of  
345 individual HPDE bearing pads of typical thickness ( $t = 20$  mm) taken to large strains is  
346 sigmoidal shaped. For 20 mm-thick bearing pads manufactured from EPDM, the compression  
347 behavior at large strains is better captured by a bilinear stress-strain hardening model (**Figure 3**).

348

349 **Figure 10** reproduces results of numerical calculations similar to those in **Figure 7** but adopting  
350 the bilinear (EPDM) and trilinear (HDPE) compressive stress-strain approximations to the  
351 measured data in **Figure 3**. Comparison of **Figure 10** with **Figure 7** shows that in many cases  
352 the gap thicknesses using the linear compressive stress-strain model are similar or smaller.  
353 Hence, using the simpler linear model will give similar or more conservative (safer) design  
354 outcomes. The exceptions are some scenarios with 2 or 4 HDPE bearing pads in combination  
355 with relative joint stiffness values greater than about 0.5 and 5, and relatively stiff and soft  
356 backfill soil cases, respectively. However, for these cases simply increasing the number of HDPE  
357 pads per joint to 6 pieces will return the joint compression response to the initial linear behavior  
358 and thus the two figures will give the same predictions.

359

## 360 **Conclusions**

361

362 The concrete panels that form the facing of steel reinforced soil walls must carry loads that are  
363 greater than the self-weight of the panels. The vertical load carried by the facing will result in  
364 compression of the horizontal joints between adjoining panels. Excessive vertical loads and/or  
365 excessively compliant bearing pads can lead to panel to panel contact which can cause the  
366 concrete panels to crack or spall.

367

368 This paper extends the work of **Damians et al. (2013)** by quantitatively investigating the  
369 influence of wall height, backfill soil constitutive model and bearing pad compression model on  
370 numerical predictions of vertical panel loads and gap compression. Rather than attempt to  
371 associate a particular value of elastic modulus with a particular soil type, which is problematic  
372 for frictional soils, a wide range of soil stiffness values spanning two orders of magnitude was  
373 used to capture the possible influence of foundation modulus on wall facing response. The  
374 numerical results show that the backfill soil stiffness, foundation compressibility and horizontal  
375 joint stiffness all influence the magnitude and distribution of vertical load through the height of  
376 the wall and bearing pad compression. The current study demonstrates that qualitative trends in  
377 vertical load factor are preserved when a more advanced stress-dependent stiffness soil  
378 hardening model is used for the backfill soil compared to the simpler linear-elastic Mohr-

379 Coulomb model. There are detectable higher vertical loads through the concrete facing panels  
380 and more gap compression in some cases using the advanced backfill soil model, but the  
381 differences are small and thus judged not to be of practical concern.

382

383 Despite the influence of many factors on the magnitude of vertical facing load and joint  
384 compression, a set of design charts was developed that can be used to select the number and type  
385 of bearing pads placed at the horizontal joints between the concrete panels so that gap closure is  
386 restricted to tolerable amounts and vertical loads transmitted through the concrete panels are not  
387 excessive. Additional analysis results are presented as design charts that can be used to estimate  
388 the settlement at the top of the concrete facing units. These charts demonstrate that settlement of  
389 the concrete facing is most sensitive to the compressibility of the foundation soil.

390

391 An important caveat to the results presented here is that only vertical facing loads and uniform  
392 joint compression are considered. In actual walls there is also the possibility of differential  
393 settlements along horizontal joints and panel tilting. These deformations can also lead to panel  
394 contact and subsequent cracking and spalling. Numerical modelling of the type used in this  
395 investigation is not a practical approach to investigate these potential but infrequent modes of  
396 failure. Rather, these types of problems are best prevented through good construction quality  
397 control including careful initial alignment of the bottom row of panels on a level and well-  
398 supported footing.

399

400

**401 Acknowledgments**

402

403 The authors wish to acknowledge the support of the Universitat Politècnica de Catalunya-  
404 BarcelonaTech (UPC) and the funding received through the research projects BIA2010-20789-  
405 C04-01 from the Ministry of Education and Innovation and CTM2013-47067-C2-1-R from the  
406 Ministry of Economy and Competitiveness of Spain.

407

408

409 **REFERENCES**

410

411 American Association of State Highway and Transportation Officials (AASHTO) (2014). LRFD  
412 Bridge Design Specifications. 7th edition, Washington, DC, USA.

413

414 Bathurst, R.J., Huang, B. and Allen, T.M. (2011). Load and resistance factor design (LRFD)  
415 calibration for steel grid reinforced soil walls. *Georisk*, 5(3-4): 218-228.

416

417 Berg, R.R., Christopher, B.R. and Samtani, N.C. (2009). Design and construction of  
418 mechanically stabilized earth walls and reinforced soil slopes, Vol. I. National Highway Institute,  
419 Federal Highway Administration, U.S. Department of Transportation, Washington, DC.

420

421 Bowles, J.E. (1996). *Foundation analysis and design*. 5th Ed., McGraw Hill, New York.

422

423 BSI (British Standards Institution). (2010). *Code of Practice for Strengthened/Reinforced Soil  
424 and Other Fills*. BSI, Milton Keynes, UK, BS 8006.

425

426 Choufani, C., Wu, P., Gagnon, G. and Macintosh, M. (2011). A precast faced mechanical  
427 stabilized earth solution for a 20 metre high mining crusher wall with various technical and site  
428 challenges. In CD proceedings of 2011 Pan-Am Canadian Geotechnical Conference, Toronto,  
429 Canada, Paper 625, 6 p.

430

431 Damians, I.P., Bathurst, R.J., Josa, A., Lloret, A. and Albuquerque, P.J.R. (2013). Vertical facing  
432 loads in steel reinforced soil walls. *ASCE Journal of Geotechnical and Geoenvironmental  
433 Engineering*, 139(9): 1419-1432.

434

435 Damians, I.P., Bathurst, R.J., Josa, A. and Lloret, A. (2014). Numerical study of the influence of  
436 foundation compressibility and reinforcement stiffness on the behavior of reinforced soil walls.  
437 *International Journal of Geotechnical Engineering*, 8(3): 247-259.

438



- 439 Damians, I.P., Bathurst, R.J., Josa, A. and Lloret, A. (2015). Numerical analysis of an  
440 instrumented steel-reinforced soil wall. *ASCE International Journal of Geomechanics*, 15(1):  
441 04014037.  
442
- 443 Findlay, T.W. (1978). Performance of a reinforced earth structure at Granton. *Ground*  
444 *Engineering*, 2(7): 42-44.  
445
- 446 Gerber, T.M. (2012). Assessing the Long-Term Performance of Mechanically Stabilized Earth  
447 Walls. (National Cooperative Highway Research Program (NCHRP) Synthesis 437).  
448 Transportation Research Board, Washington, DC.  
449
- 450 Huang, B., Bathurst, R.J. and Allen, T.M. (2012). Load and resistance factor design (LRFD)  
451 calibration for steel strip reinforced soil walls. *ASCE Journal of Geotechnical and*  
452 *Geoenvironmental Engineering*, 138(8): 922-933.  
453
- 454 Huang, B., Bathurst, R.J. and Hatami, K. (2009). Numerical study of reinforced soil segmental  
455 walls using three different constitutive soil models. *ASCE Journal of Geotechnical and*  
456 *Geoenvironmental Engineering*, 135(10): 1486-1498.  
457
- 458 Miyata, Y. and Bathurst, R.J. (2012). Analysis and calibration of default steel strip pullout  
459 models used in Japan. *Soils and Foundations*, 52(3): 481-497.  
460
- 461 Neely, W.J. and Tan, S.L. (2010). Effects of second order design factors on the behavior of MSE  
462 walls. Earth Retention Conference 3. Earth Retaining Structures Committee of the Geo-Institute  
463 of ASCE. Geotechnical Special Publications (GSP) n. 208. In Proceedings of the 2010 Earth  
464 Retention Conference held in Bellevue, Washington, August 1-4, 2010, pp. 522-530.  
465
- 466 PLAXIS (2008). Reference Manual, 2D - Version 9.02. PLAXIS B.V., Delft University of  
467 Technology, Netherlands (<http://www.plaxis.nl/>).  
468
- 469 PLAXIS (2012). Material models manual, Plaxis. Delft Univ. of Technology, Delft, Netherlands.

- 470 Runser, D.J., Fox, P.J. and Bourdeau, P.L. (2001). Field performance of a 17 m-high reinforced  
471 soil retaining wall. *Geosynthetics International*, 8(5): 367-391.  
472
- 473 Schlosser, F. and Elias, V. (1978). Friction in reinforced earth. In *Proceedings of ASCE*  
474 *Symposium on Earth Reinforcement*, Pittsburgh, PA, USA, pp. 735-763.  
475
- 476 Yu, Y., Bathurst, R.J. and Miyata, Y. (2015a). Numerical analysis of a mechanically stabilized  
477 earth wall reinforced with steel strips. *Soils and Foundations* 55(3): 536–547.  
478
- 479 Yu, Y., Damians, I.P. and Bathurst, R.J. (2015b). Influence of choice of FLAC and PLAXIS  
480 interface models on reinforced soil-structure interactions. *Computers and Geotechnics*, 65:164-  
481 174.  
482

483

484 **Table 1.** Soil properties.

Parameters	Backfill		Foundation
Unit weight (kN/m <sup>3</sup> )	19		18
Cohesion (kPa) <sup>(1)</sup>	5 <sup>(2)</sup>		50
Friction angle, $\phi$ (degrees)	36 <sup>(3)</sup>		30
Dilatancy angle, $\psi$ (degrees) <sup>(4)</sup>	6		0
Elastic Mohr-Coulomb soil model:	< 1.0 m from facing <sup>(5)</sup>	> 1.0 m from facing	
Elastic modulus (MPa)	- soft case: 5 - stiff case: 50	- soft case: 10 - stiff case: 100	- soft case: 10 - stiff case: 1000
Poisson's ratio (-)	0.3		0.3
Hardening soil model: <sup>(6)</sup>	(m = 0.5 and R <sub>f</sub> = 0.9) <sup>(7)</sup>		
E <sub>50</sub> <sup>ref</sup> (MPa) <sup>(8)</sup>	- soft case: 5 - stiff case: 50	- soft case: 10 - stiff case: 100	n/a
Poisson's ratio (-)	0.2		n/a

485

486 <sup>(1)</sup> Soils are assumed as no-tension materials (tension cut-off).487 <sup>(2)</sup> Non-zero cohesion value has been assumed for the numerical model to ensure numerical stability at very low  
488 confining pressure.489 <sup>(3)</sup> Peak plane strain friction angle of granular soil is greater than the corresponding triaxial or direct shear test  
490 values. Hence, value of  $\phi = 36$  degrees used in simulations is in agreement with conventional triaxial  
491 compression or direct shear peak friction angles of (say) 30 to 34 degrees. The latter are minimum  
492 recommended friction angles for select granular fills in North American practice (**Berg et al. 2009**).493 <sup>(4)</sup> Assumed as  $\psi = \phi - 30^\circ$ .494 <sup>(5)</sup> Area where less compaction energy is used during construction to minimize lateral loads on facing panels. The  
495 elastic stiffness modulus was assumed to be 50% of the elastic stiffness modulus of the well-compacted soil for  
496 both linear elastic Mohr-Coulomb and hardening soil model cases.497 <sup>(6)</sup> Dilatancy and dilation angle are included in hardening model.498 <sup>(7)</sup> m = 0.5 is the power term for stress-level dependency of soil stiffness and the value used here is typical for  
499 sand soils. R<sub>f</sub> corresponds to the failure ratio between the ultimate deviatoric stress and the asymptotic value of  
500 the shear strength.501 <sup>(8)</sup> E<sub>50</sub><sup>ref</sup> corresponds to the reference confining stress-dependent stiffness modulus for primary triaxial loading,  
502 corresponding to the secant stiffness at a deviatoric stress level equal to half the failure stress. Reference  
503 confining stress = 100 kPa. The unloading and reloading stiffness modulus (E<sub>ur</sub><sup>ref</sup>) was assumed to be 3 times  
504 higher than E<sub>50</sub><sup>ref</sup> which is the default assumption in the PLAXIS manual. The tangent stiffness for primary  
505 oedometer loading (E<sub>oed</sub><sup>ref</sup>) was assumed to be equal to E<sub>50</sub><sup>ref</sup>.

506

507

508

509

510

511

512 **Table 2.** Concrete panel and bearing pad (joint) properties.

Parameters	Panels	Bearing pads <sup>(1)</sup>					
		EPDM <sup>(2)</sup>			HDPE <sup>(3)</sup>		
		number of pads per panel joint					
		2	4	6	2	4	6
Axial stiffness, $J = EA$ (kN/m)	$5600 \times 10^3$	130	260	390	1100	2200	3300
Bending stiffness, $EI$ (kN/m <sup>2</sup> /m)	9150	0.25	0.50	0.75	2.10	4.20	6.20
Poisson's ratio	0.15	0.49			0.40		

513 <sup>(1)</sup> assuming a pad plan dimension area of 0.008 m<sup>2</sup> for both material cases, and a panel width 1.5 m in the running  
514 length direction of the wall and pad thickness of  $t = 20$  mm.

515 <sup>(2)</sup> EPDM = ethylene propylene diene monomer.

516 <sup>(3)</sup> HDPE = high-density polyethylene.

517

518

519

520 **Table 3.** Reinforcement layer stiffness.

Wall height, H (m)	Reinforcement layer location, depth from top of wall, z (m)	Linear-elastic stiffness, $J_{(\text{reinforcement})} = (EA)_{\text{reinforcement}}$ (MN/m)
6	0.4 to 5.3	28.1
12	0.4 to 6.4	28.1
	7.1 to 8.6	37.5
	9.4 to 10.9	46.9
	11.6	56.3
18	0.4 to 7.1	29.3
	7.9 to 11.6	44.0
	12.4 to 14.6	58.6
	15.4 to 17.6	73.3
24	0.4 to 7.1	29.3
	7.9 to 11.6	44.0
	12.4 to 15.4	58.6
	16.1 to 19.1	73.3
	19.9 to 22.9	87.9
	23.6	102.6

521

522 Notes: E = elastic modulus of steel = 200 GPa; A = cross-section area of steel strip or bars.

523

524

525 **Figure 1.** Vertical load in concrete panel wall face and gap compression. Note: Some panel  
526 systems have a lip at the back and front of the panel joint.

527

528 **Figure 2.** Finite element model geometry.

529

530 **Figure 3.** Horizontal joint compressive stress-strain behavior of EPDM and HDPE pad materials.  
531 Note: EPDM = ethylene propylene diene monomer; HDPE = high-density polyethylene.

532

533 **Figure 4.** Vertical load factor versus joint depth for different wall height (H) and backfill-  
534 foundation stiffness combinations, and assuming two 20 mm-thick bearing pads (EPDM or  
535 HDPE) per 1.5 m-long joint with linear axial (compressive) stiffness. Note: Numerical results  
536 using linear elastic M-C soil model.

537

538 **Figure 5.** Comparison of numerical results using PLAXIS hardening soil model and linear  
539 elastic M-C soil model for backfill soil. Vertical load factor versus joint depth for different wall  
540 height (H) and backfill-foundation stiffness combinations, and assuming two 20 mm-thick  
541 bearing pads (EPDM or HDPE) per 1.5 m-long joint with linear axial (compressive) stiffness.

542

543 **Figure 6.** Load factor versus relative joint stiffness. Note: Parameter z is depth of horizontal  
544 joint from top of wall.

545

546 **Figure 7.** Joint gap thickness and compression (at location of bearing pads) versus relative joint  
547 stiffness for different normalized depths of joint below top of wall ( $z/H$ ) using linear bearing pad  
548 compressive stress-strain models.

549

550 **Figure 8.** Isolines of joint vertical gap thickness for different wall height  $H$ , joint stiffness  
551 (different numbers of bearing pads per joint), and different backfill soil and foundation stiffness  
552 conditions. Wall heights:  $H = 6$  m (a),  $H = 12$  m (b),  $H = 18$  m (c), and  $H = 24$  m (d).

553

554 **Figure 9.** Influence of wall height, soil backfill and foundation stiffness, bearing pad type and  
555 number on settlement at the top of the concrete panel facing.

556

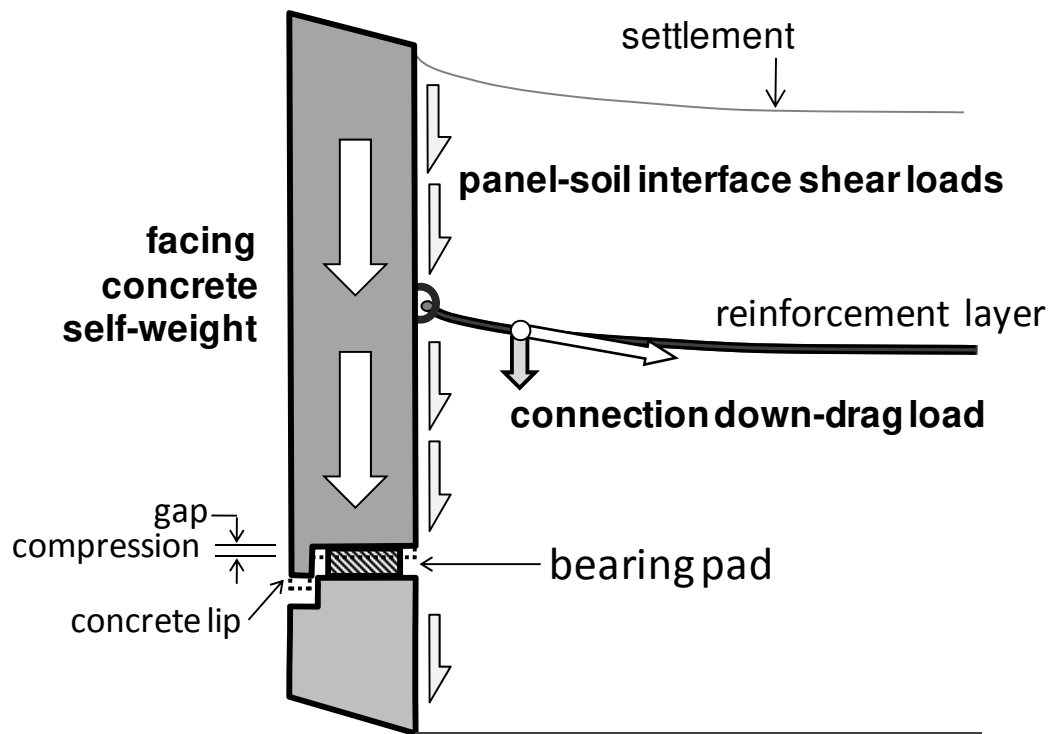
557 **Figure 10.** Joint gap thickness and compression versus relative joint stiffness for different  
558 normalized depths of joint below top of wall ( $z/H$ ) using bilinear (EPDM) and trilinear (HDPE)  
559 bearing pad compressive stress-strain models.

560

561

562

563



564

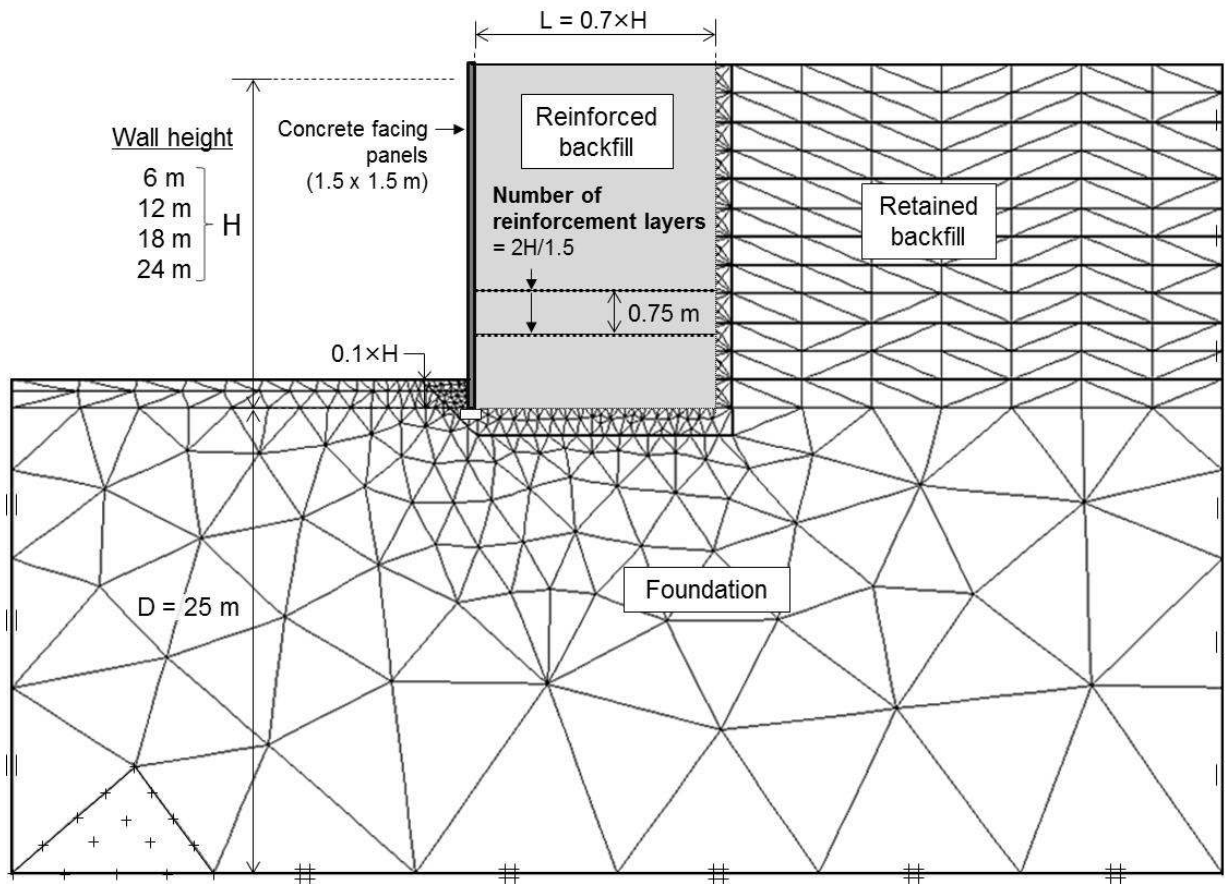
565

566 **Figure 1.** Vertical load in concrete panel wall face and gap compression. Note: Some panel  
567 systems have a lip at the back and front of the panel joint.

568

569



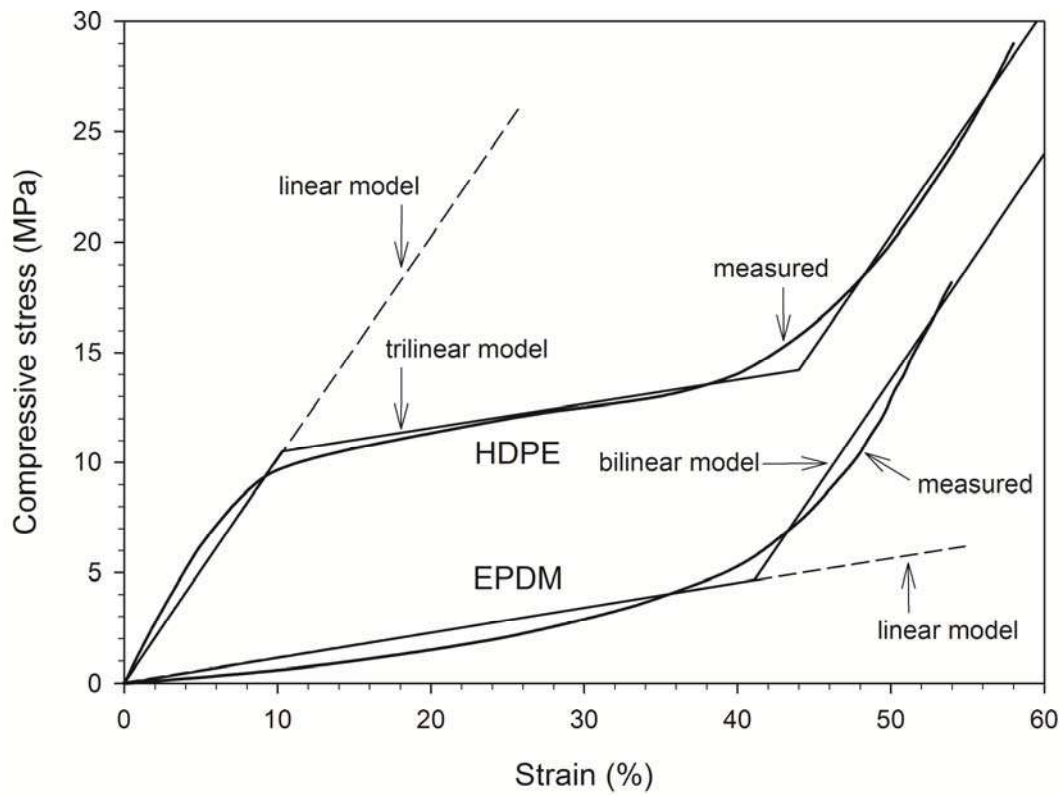


570

571

572 **Figure 2.** Finite element model geometry.

573



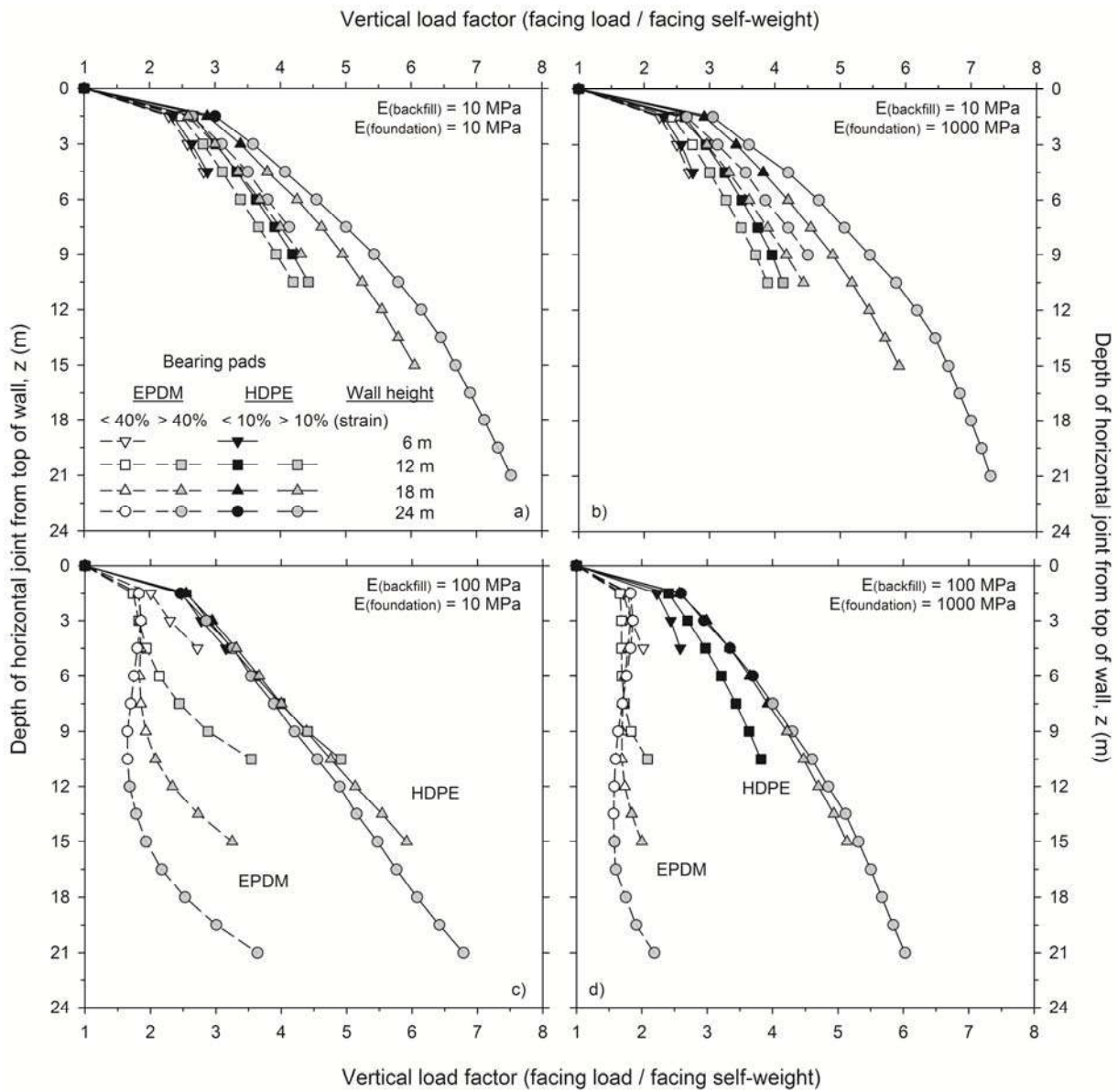
574  
575

576 **Figure 3.** Horizontal joint compressive stress-strain behavior of EPDM and HDPE pad materials.

577 Note: EPDM = ethylene propylene diene monomer; HDPE = high-density polyethylene.

578  
579  
580  
581

582



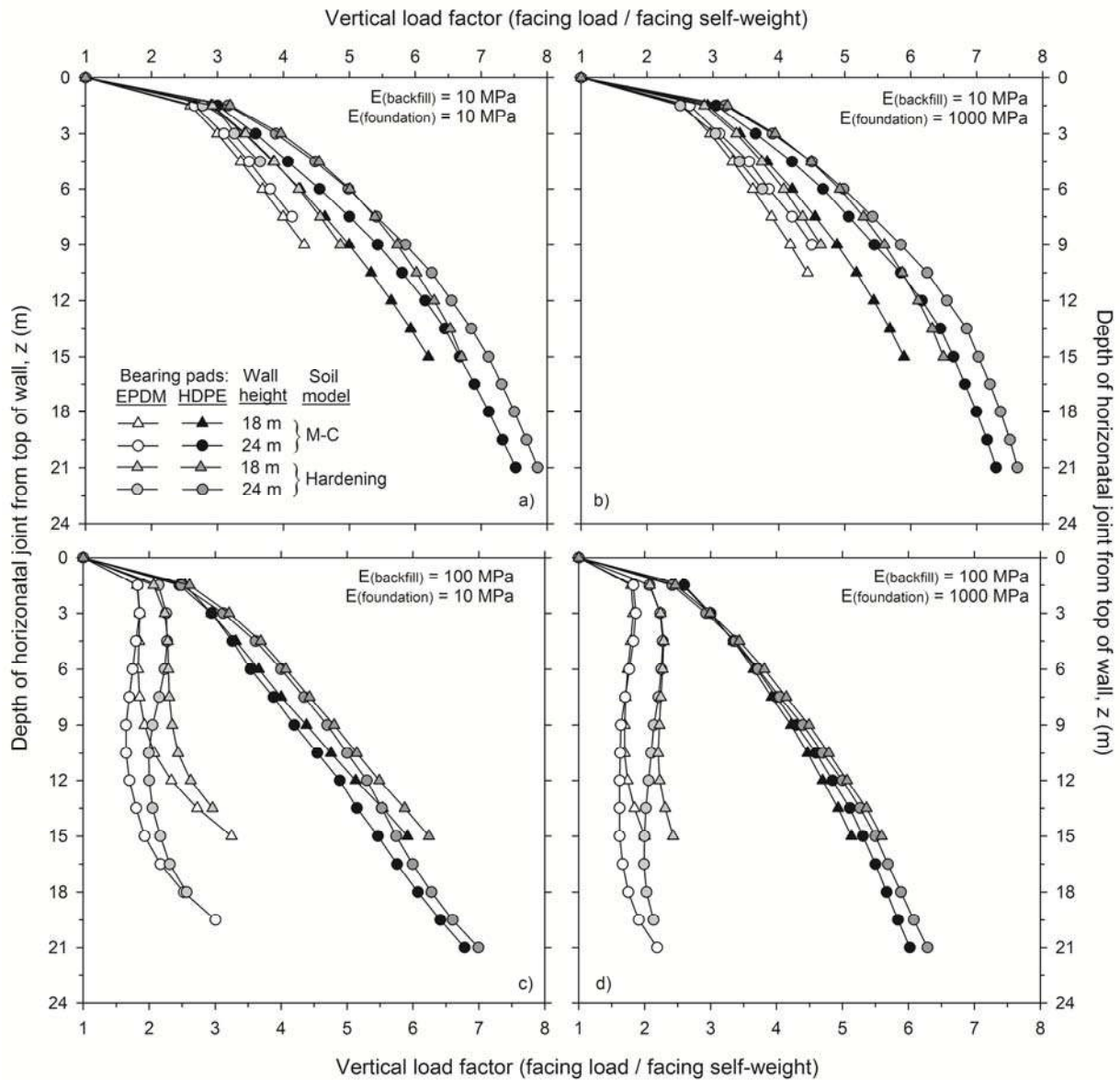
583

584

585 **Figure 4.** Vertical load factor versus joint depth for different wall height (H) and backfill-  
 586 foundation stiffness combinations, and assuming two 20 mm-thick bearing pads (EPDM or  
 587 HDPE) per 1.5 m-long joint with linear axial (compressive) stiffness. Note: Numerical results  
 588 using linear elastic M-C soil model.

589

590



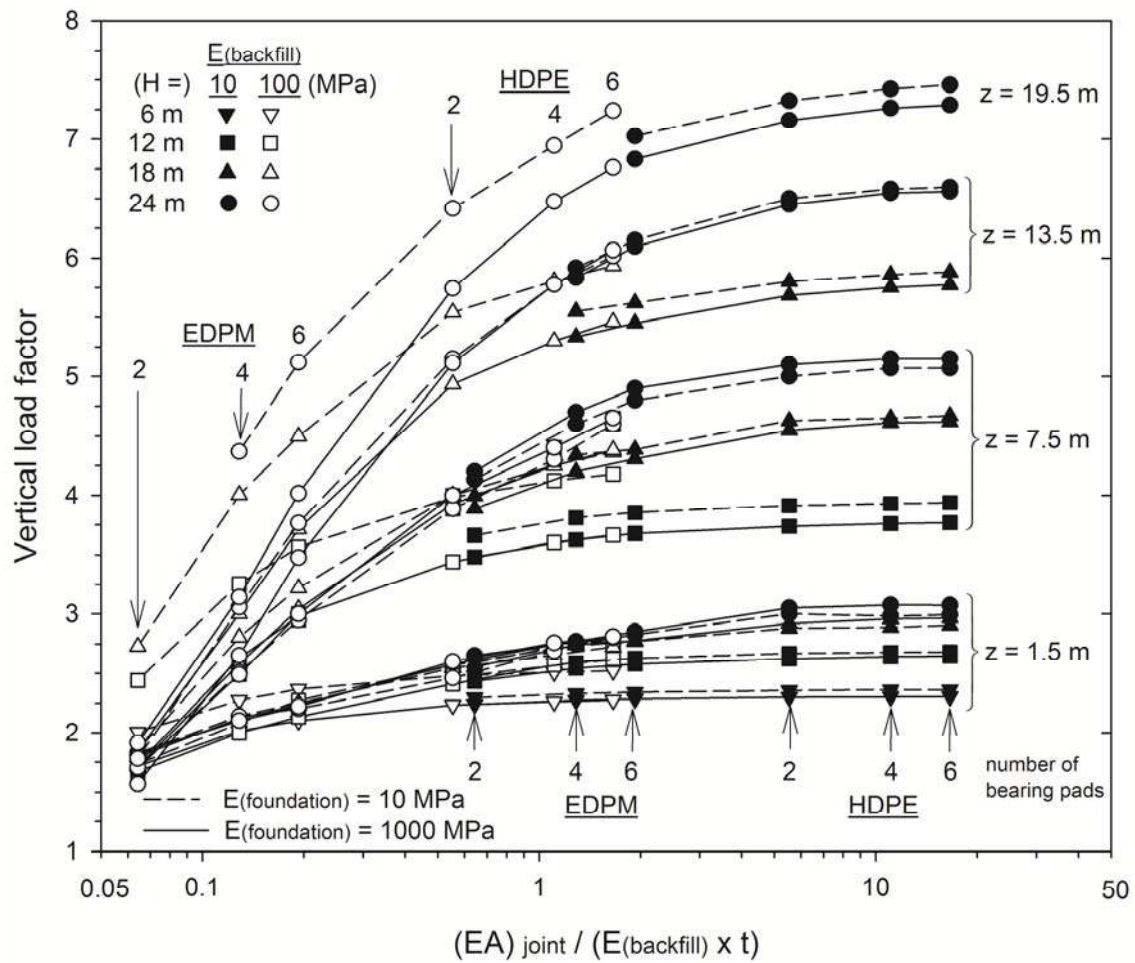
591

592

593 **Figure 5.** Comparison of numerical results using PLAXIS hardening soil model and linear  
 594 elastic M-C soil model for backfill soil. Vertical load factor versus joint depth for different wall  
 595 height (H) and backfill-foundation stiffness combinations, and assuming two 20 mm-thick  
 596 bearing pads (EPDM or HDPE) per 1.5 m-long joint with linear axial (compressive) stiffness.

597

598

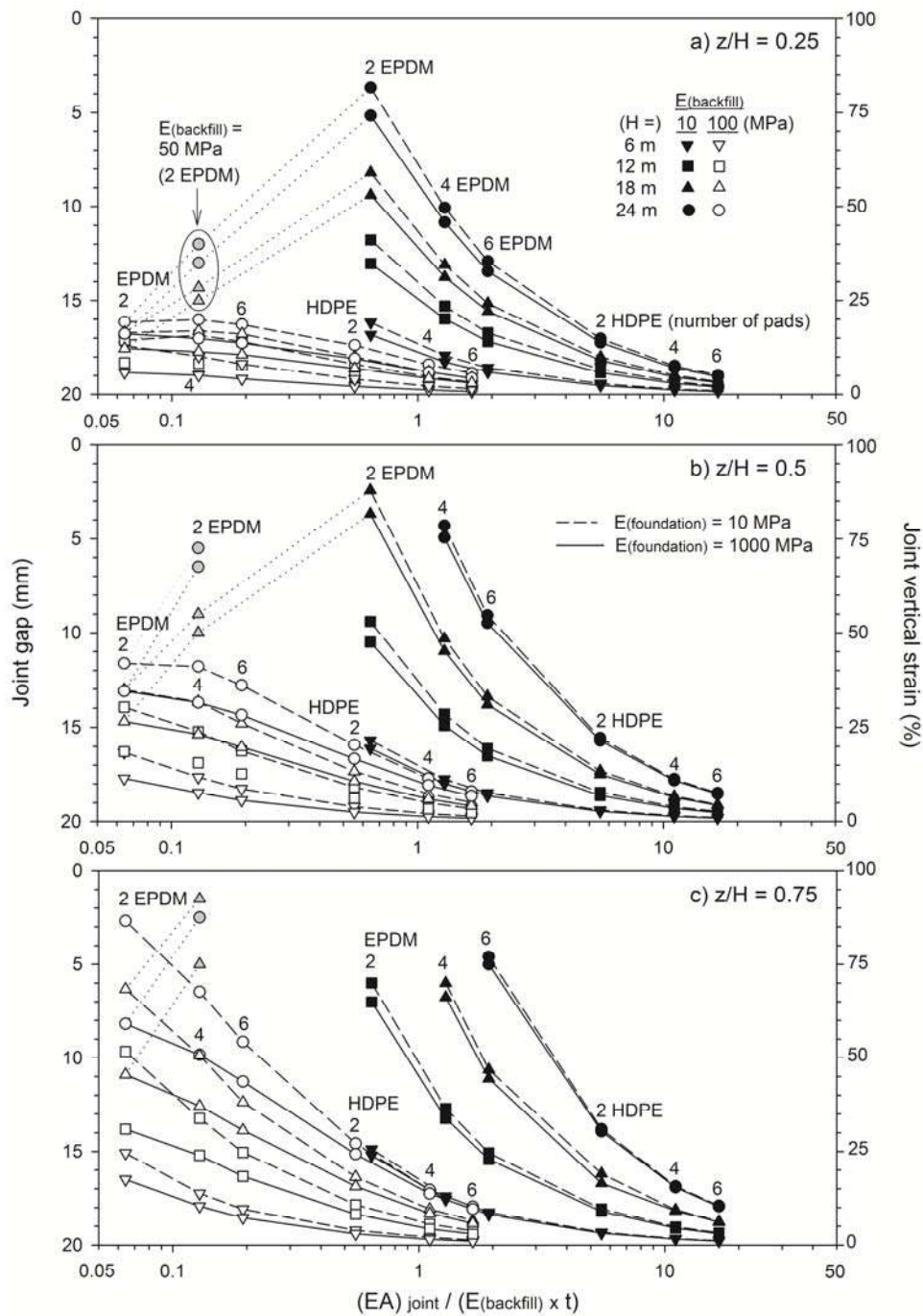


599

600

601 **Figure 6.** Load factor versus relative joint stiffness. Note: Parameter z is depth of horizontal  
 602 joint from top of wall.

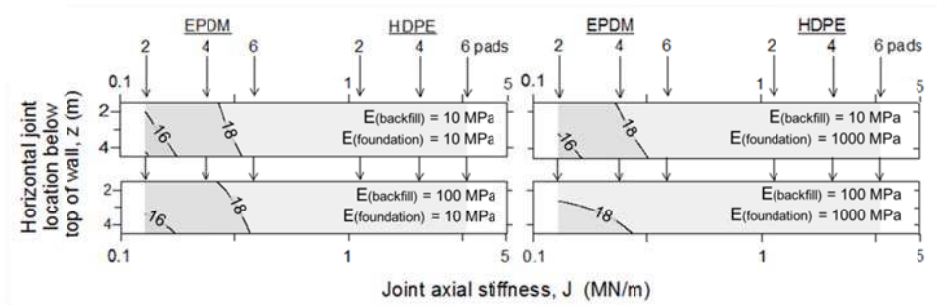
603



604

605 **Figure 7.** Joint gap thickness and compression (at location of bearing pads) versus relative joint  
 606 stiffness for different normalized depths of joint below top of wall ( $z/H$ ) using linear bearing pad  
 607 compressive stress-strain models.

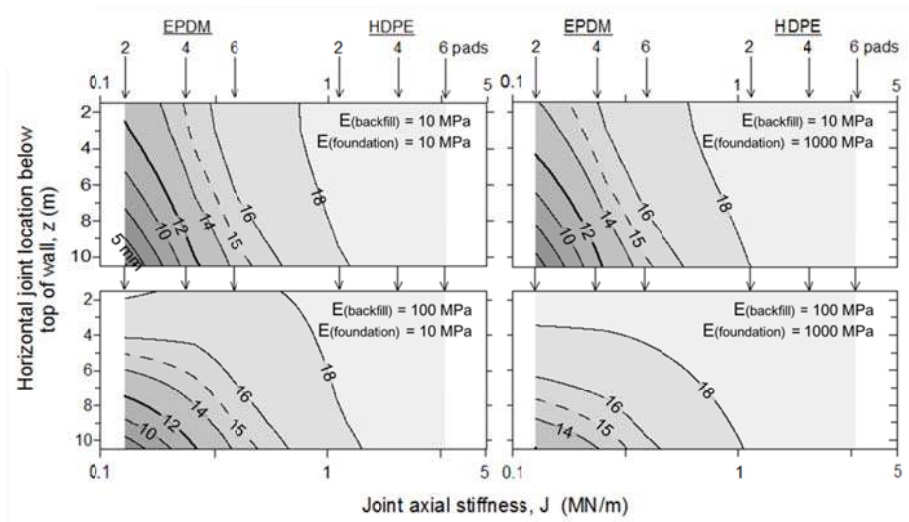
608 a) H = 6 m



609  
610  
611  
612  
613  
614

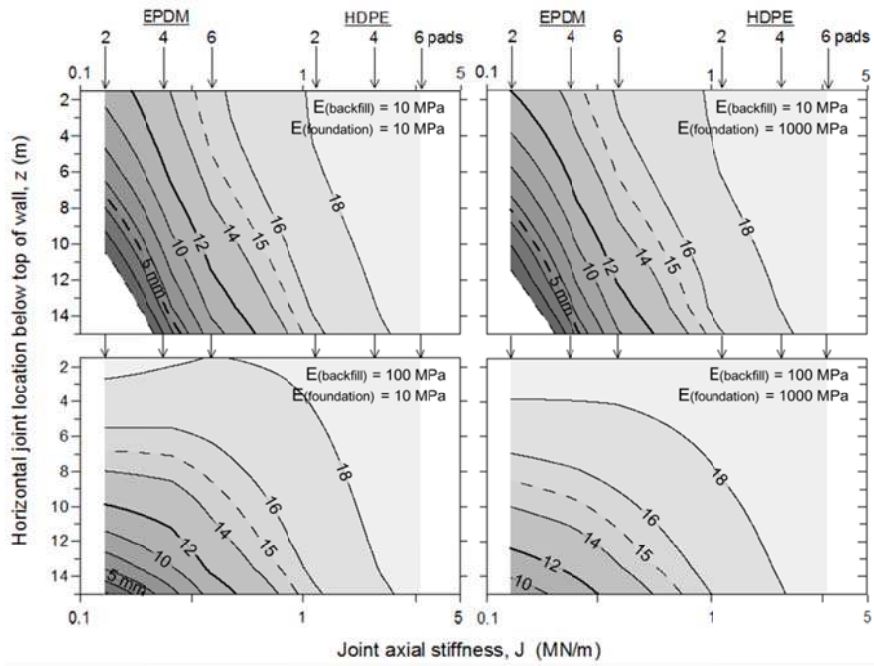
615 b) H = 12 m

616



617

618 c)  $H = 18$  m

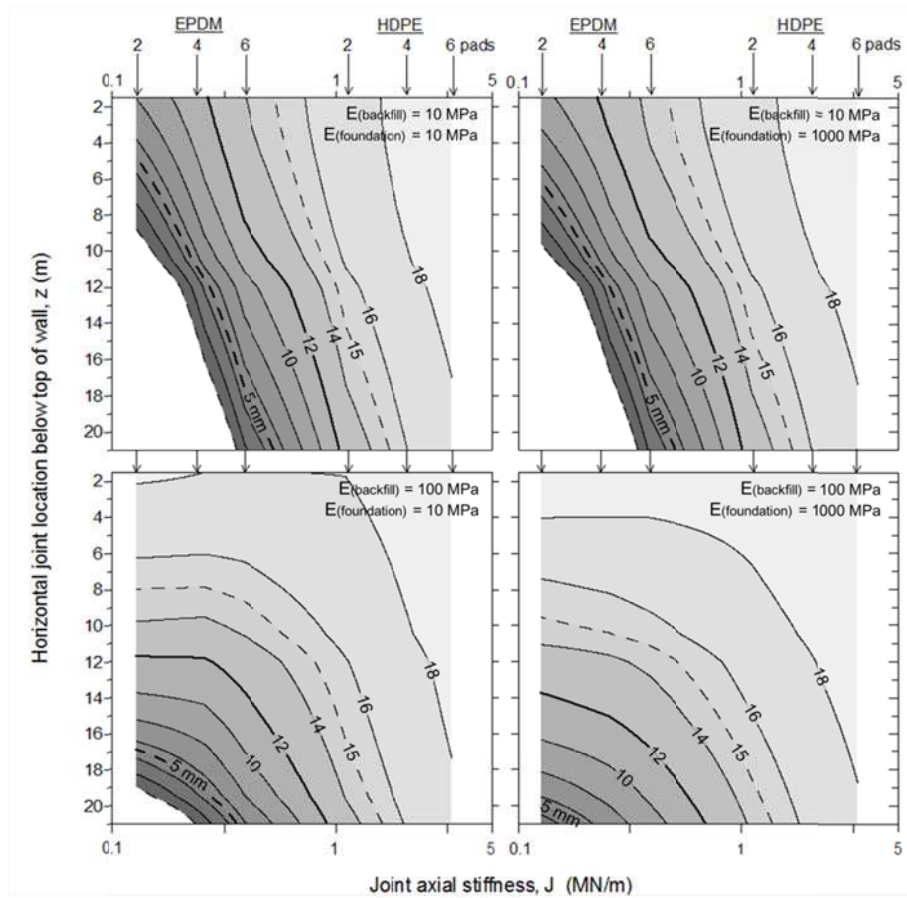


619  
620



621 d)  $H = 24$  m

622

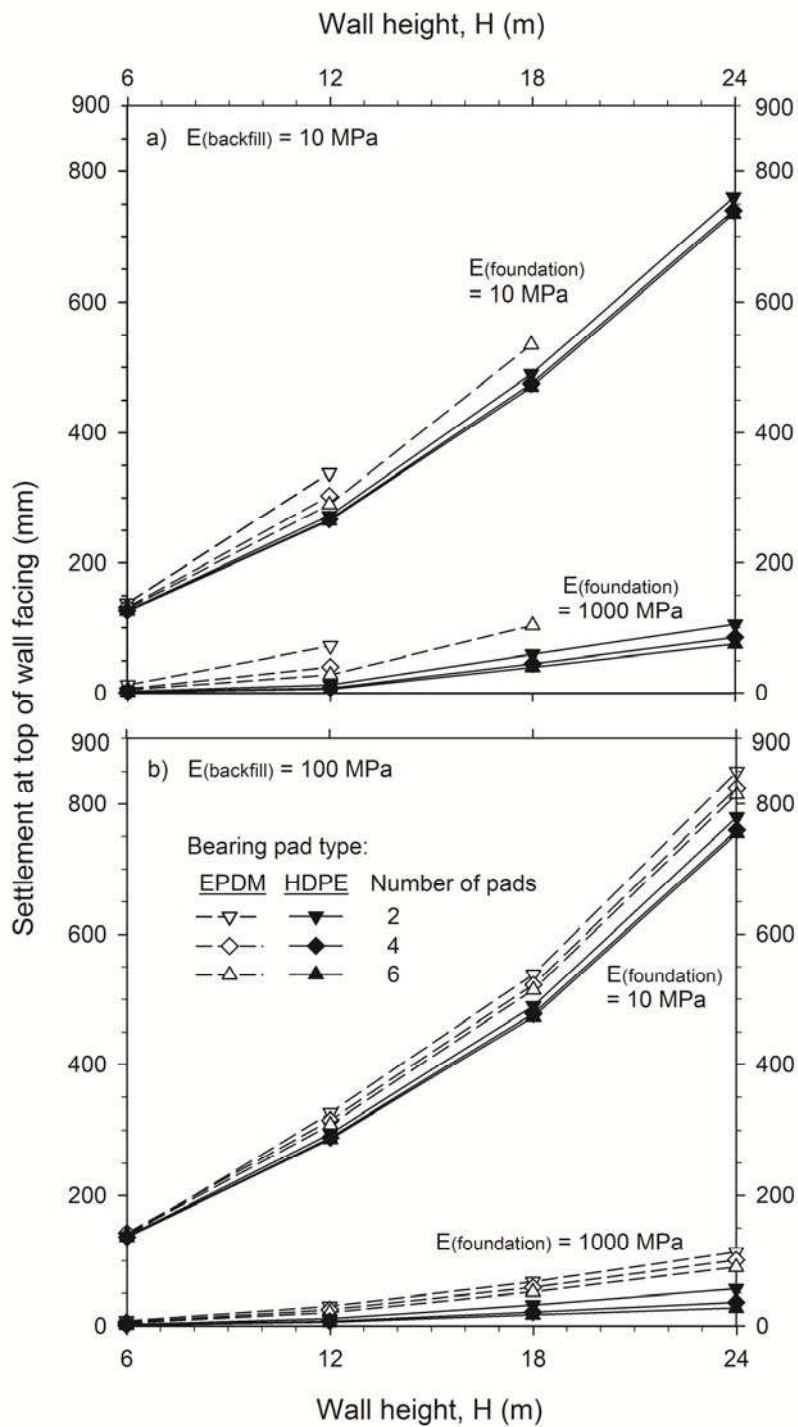


623

624

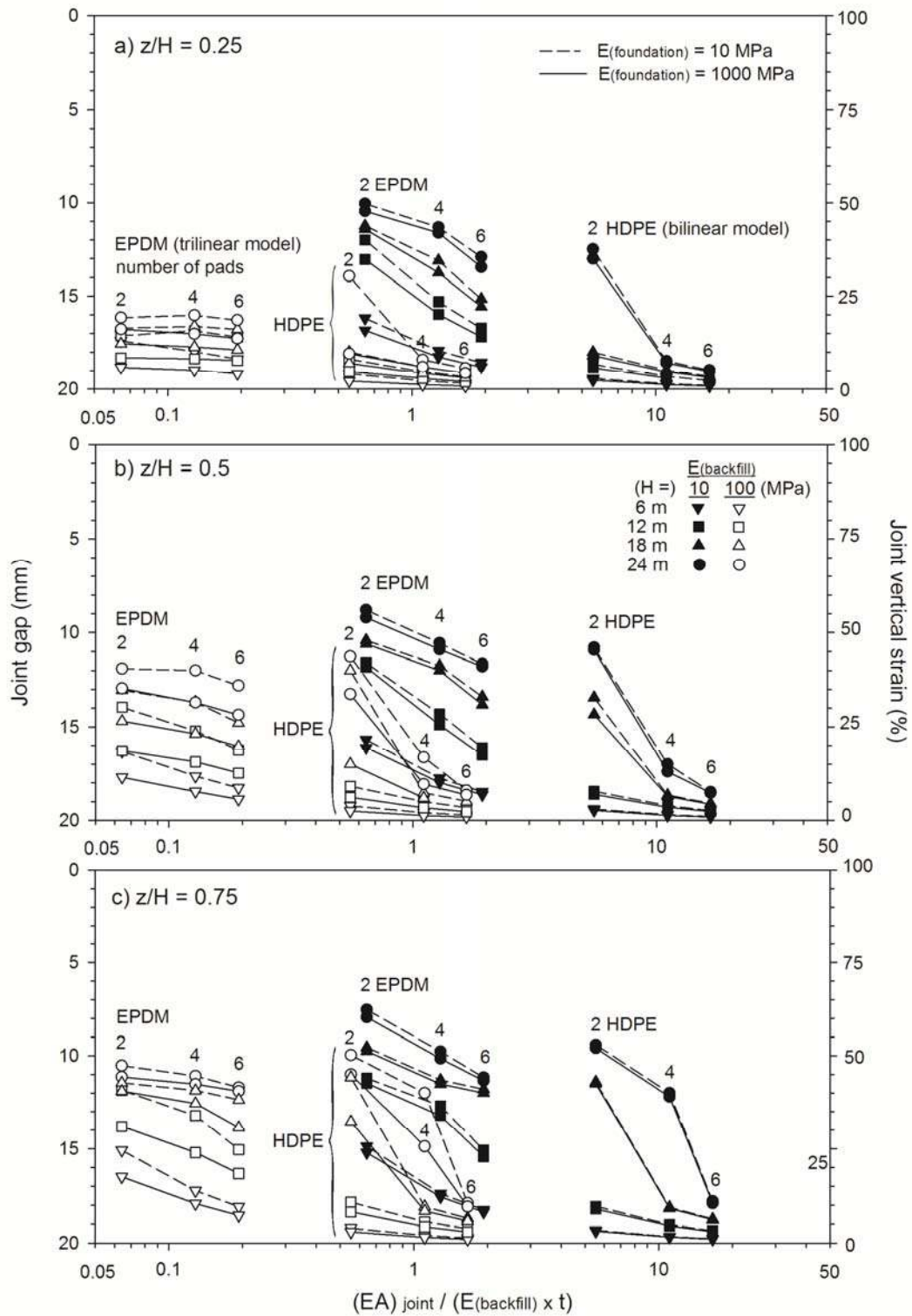
625 **Figure 8.** Isolines of joint vertical gap thickness for different wall height  $H$ , joint stiffness  
 626 (different numbers of bearing pads per joint), and different backfill soil and foundation stiffness  
 627 conditions. Wall heights:  $H = 6$  m (a),  $H = 12$  m (b),  $H = 18$  m (c), and  $H = 24$  m (d).

628



629

630 **Figure 9.** Influence of wall height, soil backfill and foundation stiffness, bearing pad type and  
 631 number on settlement at the top of the concrete panel facing.



632

633 **Figure 10.** Joint gap thickness and compression versus relative joint stiffness for different  
 634 normalized depths of joint below top of wall ( $z/H$ ) using bilinear (EPDM) and trilinear (HDPE)  
 635 bearing pad compressive stress-strain models.